FATIGUE ANALYSIS OF STOCHASTIC SYSTEMS SUBJECTED TO CYCLIC LOADING IN THE FREQUENCY DOMAIN

U. L. Rosa [1], A. M. G. Lima [2]

Federal University of Uberlândia, School of Mechanical Engineering, Campus Santa Mônica, 38400-902, Uberlândia, MG, Brazil

[1] ulisses.ufu@hotmail.com

[2] amglima@mecanica.ufu.br

Abstract: The design of engineering systems depends on a number of factors, highlighting the environment where it will work and how it will be loaded. The greatest part of tests concerning stresses do not approximate real conditions that most of them are subjected. In the analysis of materials charged with random loadings, the major problem is the material failure by fatigue that occurs with no previous notice and generally on a sudden and catastrophic way. On this case, the characterization of the phenomenon requires application of statistical methods and determination of non-static properties. The interest of this contribution is to describe fatigue in thin plates considering the existence of uncertainties concerned to the structure itself, such as variations on material's elastic properties and geometry. An exact stochastic finite elements method with its discretization obtained by the application of Karhunen-Loève expansions method is developed. Fatigue damage is estimated by the Sines criterion and Monte Carlo Simulation (MCS) combined with Latin Hypercube Sampling is used as the stochastic solver. This process requires stress analysis on Fourier's domain, generating power spectral densities (PSD) of the structure submitted to random loadings. After the theoretical developments, the numerical results obtained by using a thin plate subjected to random multiaxial Gaussian loads are presented.

Keywords: fatigue, random vibrations, stress PSD, Sines criterion, finite elements method

INTRODUCTION

In the development of mechanical structures, there are several points that require attention from engineers. Subjective concepts such as comfort and cost are very important for buyers and customers but parameters like safety and reliability must always be considered in projects. In the context of fatigue analysis, safety and reliability implies on crack propagation control and prevention.

Dimensioning a structure for static loadings is not a complex process since the modulus and limits are available for most materials. On the other hand, if there is any kind of random or variable loading actuating, the generated stresses vary with time or fluctuate between levels and so the fatigue phenomenon starts to be a problem because its failure maximum stresses are below the material's ultimate strength and even bellow its yield strength (Budynas and Nisbett, 2011). Besides charging fluctuations, the structure's material properties and its geometry may be uncertain. In other words, values found on literature and given by manufacturers are not always the exact real values measured.

Fatigue is caused by generation and propagation of cracks and is accelerated by effects of environment and frequency of cycling. Dowling (2007) said that this phenomenon's biggest problem is that it occurs generally on a very dangerous, sudden and catastrophic way, without previous notice. Lambert (2007) pointed out that fatigue cracks usually appear on critical points where the stress levels are higher but remarked that working on time domain analyzing stress historic is possible but impracticable due to high time spent on data acquisition and post treatment. Therefore, the viable way is to obtain data from frequency domain, specifically by statistical analysis of the structure's stress spectral power density (stress PSD).

Weber (1999) studied several fatigue criteria and their formulations and concluded that Sines' criterion is the one that better includes accuracy and has a simple formulation. Sines (1959) proposed a stress criterion for multiaxial fatigue that consists on the calculation of a factor that is function of the square root of the stress deviation tensor second invariant, the hydrostatic stresses and material parameters related to fatigue tests. The method developed by Li and de Freitas (2002) considers the non-proportionality of the loading on the estimation of this second invariant. Its calculations involves spectral moments obtained directly from the stress PSD.

The stochastic finite element method is used to generate the exact mass and stiffness matrices of the system by applying the so named Karhunen-Loève expansion method (Ghanem and Spanos, 1991). This method guarantees the extension of aleatory effects to the whole structure and not only on the physical properties. Also, parameters chosen as random variables as factored out of the matrices. Monte Carlo Simulation (MCS) (Rubinstein, 1981) combined with Latin Hypercube Sampling (LHC) is used as the stochastic solver (Florian, 1992).

FINITE ELEMENTS FORMULATION FOR STRESS ANALYSIS

The objective of this section is to present the formulation of the deterministic finite elements method. The term deterministic in this case means that are no aleatory effects comprised in this analysis. Because of this, in this problem's first approach, mean values are used in the stiffness and mass matrices calculation. First, the classical finite elements method was used to obtain the nodal displacement field. The concerned structure is a thin plate sized $0.654m \times 0.527m$ and the discretization used in the modeling is a 12×12 plane rectangular finite elements mesh with four nodes and five degrees of freedom per node, which are three in-plane displacements in directions x, y, z (denoted by u_0, v_0, w_0) and two cross-section rotations (denoted by θ_x, θ_y) comprising a total number of 845 DOF. Double clamping along y axis is assumed as boundary conditions. The plate's mean mechanical properties are given on Tab. 1 and a simplified schema regarding its axis and meshing is depicted in Fig. 1.

Table 1. Mechanical properties of the aluminum plate

Thickness (mm)	Young's Module (GPa)	Poisson ratio	Mass density (kg/m³)	Ultimate strength limit (MPa)	Alternate torsional limit[1] (MPa)	Alternate traction limit[1] (MPa)
1.5	70	0.33	2700	343	92	132

[1]obtained for 2.0×10^6 cycles

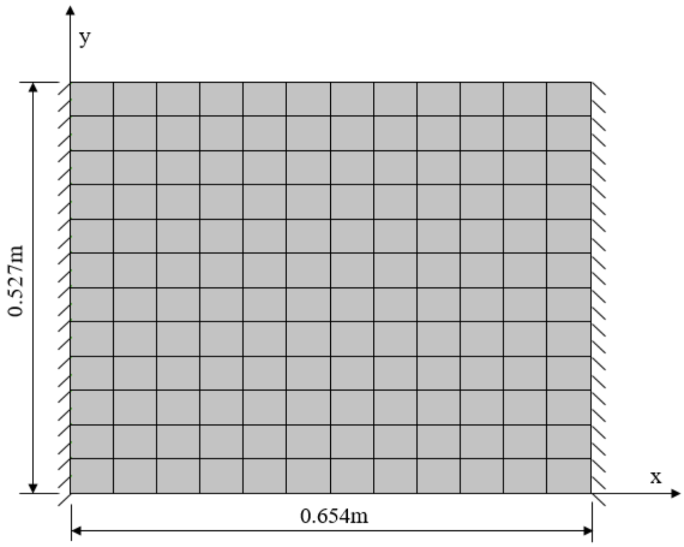

Figure 1. Thin plate simplified schema and meshing

The thin plate model is obtained by Kirchhoff's theory (Zienkiewicz and Taylor, 2005). The displacement fields are given by Eq. (1).

$$\mathbf{u}(x,y,z,t) = u_0 + z\theta_x \tag{1.a}$$

$$\mathbf{v}(x,y,z,t) = v_0 + z\theta_y \tag{1.b}$$

$$\mathbf{w}(x,y,z,t) = w_0 \tag{1.c}$$

All the structures degrees of freedom (elements on the right side of the equations) are approximated by shape functions denoted $\boldsymbol{N}(x,y)$ as shown on Eq. (2).

$$\begin{Bmatrix} \mathbf{u}(x,y,z,t) \\ \mathbf{v}(x,y,z,t) \\ \mathbf{w}(x,y,z,t) \end{Bmatrix} = \mathbf{U}(x,y,z,t) = \mathbf{A}(z)\mathbf{N}(x,y)\mathbf{u_e}(t) \tag{2}$$

where $\boldsymbol{A}(z)$ is a matrix containing the parameter z and $\boldsymbol{u_e}(t)$ is the nodal displacement data vector.

From now on, the continuous system will be represented by the discretization mentioned above. Shape functions are used to calculate stiffness and mass properties of the system. Discretized, this matrices are square, symmetric and their size is the DOF number. The calculation of these two matrixes follow developments based on energy variational approaches (kinetic energy for the mass and potential energy for stiffness) applied on FEM models. Formulation for elementary matrices are presented on Eq. (3) and (4) and are lately assembled by the system's connectivity, composing the global matrices shown on Eq. (5) and (6) (Faria, 2006).

$$\mathbf{M}^{(e)} = \int_{V_e} \rho \boldsymbol{N}(x,y)^T \boldsymbol{N}(x,y) dV_e \tag{3}$$

$$\mathbf{K}^{(e)} = \frac{1}{2} \int_{Ve} \dot{\boldsymbol{N}}(x,y)^T \,\mathbf{H}\, \dot{\boldsymbol{N}}(x,y)\, dV_e \tag{4}$$

where $\mathbf{H}$ is the mechanical properties matrix, depending on the structure's material.

$$\mathbf{M} = \bigcup_{i=1}^{n} \mathbf{M}_i^{(e)} \tag{5}$$

$$\mathbf{K} = \bigcup_{i=1}^{n} \mathbf{K}_i^{(e)} \tag{6}$$

where n is the number of elements.

Now it is possible to write the system's movement ordinary differential equation. Equation (7) governs the undamped structure's movement and its solution estimates the displacement field.

$$\mathbf{M}\ddot{\mathbf{U}} + \mathbf{K}\mathbf{U} = \mathbf{F} \tag{7}$$

where $\mathbf{F}$ is an external load applied to the system.

By assuming that the displacement fields have been determined by performing Eq. (7), it is possible to obtain strain fields formulation. They are related to $\mathbf{U}(x,y,z,t)$ by the use of derivatives shown on Eq. (8).

$$\begin{Bmatrix} \varepsilon_x \\ \varepsilon_y \\ \gamma_{xy} \end{Bmatrix} = \begin{bmatrix} \partial/\partial x & 0 & 0 \\ 0 & \partial/\partial y & 0 \\ \partial/\partial y & \partial/\partial x & 0 \end{bmatrix} \begin{Bmatrix} u \\ v \\ w \end{Bmatrix} = \mathbf{D}\,\mathbf{U}(x,y,z,t) \tag{8}$$

where $\mathbf{D}$ is the differential matrix and $\boldsymbol{\varepsilon}(x,y,z,t)$ the elemental strain vector.

By defining the matrix $\mathbf{B}(x,y,z) = \mathbf{D}\,\mathbf{A}(z)\mathbf{N}(x,y)$, Eq. (8) is rewritten as follows:

$$\boldsymbol{\varepsilon}(x,y,z,t) = \mathbf{B}(x,y,z)\mathbf{u_e}(t) \tag{9}$$

Equation (10) represents Hooke's law application to the strain field shown on Eq. (9), obtaining the stress fields for each element of the structure.

$$\boldsymbol{\sigma}(x,y,z,t) = \mathbf{H}\boldsymbol{\varepsilon}(x,y,z,t) \tag{10}$$

Time responses acquisition demands high computational efforts, so it is highly recommended working on Fourier's frequency domain (Lambert, 2007). To a closer reality approach, it is convenient to add a structural damping to Eq. (7). For this thin plate model, it is considered as a proportional damping obtained directly from a coefficient multiplying the stiffness matrix $(\mathbf{C} = \beta\,\mathbf{K})$. Equation (11) represents the full model.

$$\mathbf{M}\ddot{\mathbf{U}} + \mathbf{C}\dot{\mathbf{U}} + \mathbf{K}\mathbf{U} = \mathbf{F} \tag{11}$$

Equation (12) represents the system's frequency response and is obtained applying Fourier's transformation to Eq. (11).

$$\mathbf{U}(\omega) = \left[-\omega^2\mathbf{M} + j\omega\mathbf{C} + \mathbf{K}\right]^{-1} \mathbf{F}(\omega) \tag{12}$$

where $\boldsymbol{U}(\omega)$ and $\boldsymbol{F}(\omega)$ are the Fourier's transform of the displacement and the applied loading, respectively.

The structure's frequency response function (FRF) is defined on Eq. (13).

$$\mathbf{G}(\omega) = \left[-\omega^2\mathbf{M} + j\omega\mathbf{C} + \mathbf{K}\right]^{-1} \tag{13}$$

The evaluation of Eq. (13) requires matrix inversions. The size of these matrices is proportional to the number of degrees of freedom and elements, making prohibitive its inversion depending on the size of the model. Lambert (2007) says that this is the main reason a modal basis is needed to solve effectively this equation. The interest on this section is defining a basis $\boldsymbol{T}$ to reduce the number of the structure's effective degrees of freedom.

Gerges (2013) pointed out several reduction methods and the best adapted to a linear thin plate is using Ritz basis. It is composed of nodal displacements of vibration modes and is enriched with static residue of a unitary load. The number of modes considered depends on the accuracy needed. The more modes inserted, the closer to reality the system is but takes more computation time. It is usual to analyze 1.5 times the desired frequency range and to consider all the n_m vibration modes inside it. For example, for a 0-100 Hz range analysis, it is recommended to work on a 0-150 Hz range and all the modes below 150 Hz must be used on the basis composition. Equation (14) represents how it is assembled.

$$\boldsymbol{T} = [\boldsymbol{U}_{LF} \ \bar{\boldsymbol{U}}] \tag{14}$$

where $\boldsymbol{U}_{LF}$ are the low frequency (first n_m modes) nodal displacements obtained by the solution of a eigenvector problem of the homogeneous equation associated to Eq. (7) and $\bar{\boldsymbol{U}}$ is the static residue due to a unitary load.

This base is applied to the other matrixes on the model, generating a completely new system that demands less computational efforts on its solution. Equation (15) shows how the reduction basis is applied.

$$\mathbf{M_R} = \boldsymbol{T}^{\mathrm{T}}\,\mathbf{M}\,\boldsymbol{T} \tag{15.a}$$

$$\mathbf{K_R} = \boldsymbol{T}^{\mathrm{T}}\,\mathbf{K}\,\boldsymbol{T} \tag{15.b}$$

where $\boldsymbol{M_R}$ and $\boldsymbol{K_R}$ are the reduced mass matrix and reduced stiffness matrix respectively. It is possible to obtain a reduced structural damping matrix the same way it is described before $\left(\mathbf{C}_{\boldsymbol{R}} = \beta\,\mathbf{K}_{\boldsymbol{R}}\right)$.

From now on for an easier writing and comprehension, calculations concerning these matrices will not have the sub index R anymore, but will always refer to the reduced model. Results concerning model reduction can be found in bibliographic reference (Rosa and de Lima, 2015).

The assumption of the existence of autocorrelation and cross-correlation functions makes possible to define spectral density functions via correlation functions (Bendat and Piersol, 2010). They are defined on the interval $(-\infty,+\infty)$ and have symmetry properties. As negative frequencies are not interesting in this analysis, it is convenient to introduce the one-sided spectral function, defined on $\left[0,+\infty\right)$. Its values are always double of the two-sided spectral function evaluated on positive frequencies. One system's power spectral density matrix of displacement $\boldsymbol{\phi}_u(\omega)$ is shown on Eq. (16).

$$\boldsymbol{\phi}_u(\omega) = \int_{-\infty}^{+\infty} \boldsymbol{R}_u(\tau) e^{-j\omega t}\, d\tau \tag{16}$$

where $\boldsymbol{R}_u$ is the autocorrelation function of the displacement field, submitted to a load *f(t)* with autocorrelation function $\boldsymbol{R}_f$. In time domain, its value is given by Eq. (17).

$$\boldsymbol{R}_u(\tau) = \int_{-\infty}^{+\infty}\int_{-\infty}^{+\infty} \boldsymbol{g}(\lambda)\,\boldsymbol{R}_f(\tau+\lambda-\zeta)\,\boldsymbol{g}^T(\zeta)\,d\lambda\, d\zeta \tag{17}$$

where $\boldsymbol{g}(t) = \frac{1}{2\pi}\int_{-\infty}^{+\infty} \boldsymbol{G}(\omega) e^{j\omega t}\, d\omega$ is the system's impulse response.

Equations (16) and (17) are rearranged using Fourier transform definitions and spectral density properties (Lambert, 2007) formulating Eq. (18), that relates the displacement PSD, load PSD $\boldsymbol{\phi}_f(\omega)$ and system's FRF.

$$\boldsymbol{\phi}_U(\omega) = \boldsymbol{G}(\omega)\left(\int_{-\infty}^{+\infty} \boldsymbol{R}_f(\tau) e^{j\omega t}\, d\tau\right)\boldsymbol{G}^H(\omega) = \boldsymbol{G}(\omega)\boldsymbol{\phi}_f(\omega)\boldsymbol{G}^H(\omega) \tag{18}$$

All the relations established for time domain on the previous sections are valid on frequency domain as well. So using Eqs. (9), (10) and (18) it is possible to write Eq. (19), that is an expression for stress PSD $\boldsymbol{\phi}_S(\omega)$.

$$\boldsymbol{\phi}_S(\omega) = \boldsymbol{H}\,\boldsymbol{B}\,\boldsymbol{G}(\omega)\,\boldsymbol{\phi}_f(\omega)\,\boldsymbol{G}^H(\omega)\,\boldsymbol{B}^T\boldsymbol{H}^T \tag{19}$$

After applying the reduction basis from Eq. (14) on Eq. (19), the reduced stress PSD for each element is obtained. It is shown on Eq. (20) where $\boldsymbol{\Psi} = \mathbf{H\,B\,T}$ are the reduced elastic properties and differential matrices, $\boldsymbol{Z}(\omega)$ is the reduced FRF calculated for each element and $\boldsymbol{\phi}_F(\omega) = \boldsymbol{T}^T\boldsymbol{\phi}_f(\omega)\boldsymbol{T}$ is the reduced load PSD.

$$\boldsymbol{\phi}_S(\omega) = \boldsymbol{\Psi}\,\boldsymbol{Z}(\omega)\,\boldsymbol{\phi}_F(\omega)\,\boldsymbol{Z}^H(\omega)\,\boldsymbol{\Psi}^T \tag{20}$$

Stochastic Finite Elements Formulation

In order to prepare the system for the inclusion of uncertain variables, a parametrization is required. The first step is to separate the stiffness and mass matrices in two effects (membrane and bending). The separation makes possible to define a group of parameters that may be subjected to fluctuations and random effects on its values and factor them out of the matrices. For this study, there were chosen the thickness t, Young modulus E and density ρ. Equations (21) and (22) present the parametrized matrices.

$$\mathbf{K} = Et\,\mathbf{K}_m + Et^3\mathbf{K}_b \tag{21}$$

$$\mathbf{M} = \rho t\,\mathbf{M}_m + \rho t^3\mathbf{M}_b \tag{22}$$

where subscripts m and b designates membrane and bending effects, respectively.

The Karhunem-Loève (KL) decomposition (or expansion) is a continuous representation for random fields expressed as the superposition of orthogonal random variables weighted by deterministic spatial functions (de Lima et al., 2010). A continuous bidimensional random field $H(x, y,\theta)$ is composed by a combination of spatial variables (x, y) and random variables (expressed by θ). Applying KL method, an approximation for the continuous random field is generated. It is shown on Eq. (23).

$$H(x, y,\theta) \cong \hat{H}(x, y,\theta) = E\left(x, y\right) + \sum_{r=1}^{n}\sqrt{\lambda_r}\, f_r(x, y)\xi(\theta) \tag{23}$$

where $E\left(x, y\right) = \varepsilon[H\left(x, y,\theta\right)]$ is the expectation operator applied to the random field, f_r and λ_r are the eigenfunctions and eigenvectors of its bidimensional covariance function and $\xi(\theta)$ is a function representing random variables. It is important to note that this expansion is truncated in $r = n$ terms.

Ghanem and Spanos (1991) proposed some functions to approximate the solution of the eigenvector problem regarding the covariance function with different shapes and properties. One of these properties, present in the exponential function, is the separability propertie. It makes possible to decouple the bidimensional problem into a combination of two unidimensional fields. The eigenvector and eigenvalue solution become $f_r\left(x, y\right) = f_i(x) f_j(y)$ and $\lambda_r = \lambda_i\lambda_j$, respectively. Equation (24) presents the exponential covariance function formulation.

$$C\left[\left(x_1, y_1\right),\left(x_2, y_2\right)\right] \cong \exp\left(-\frac{\left|x_1 - x_2\right|}{L_{cor,x}} - \frac{\left|y_1 - y_2\right|}{L_{cor,y}}\right) \tag{24}$$

where $L_{cor,x}$ and $L_{cor,y}$ are the correlation lengths defined on the geometric domains $\Omega_x = \left(x_1, x_2\right)$ and $\Omega_y = \left(y_1, y_2\right)$.

The procedures for its solution are presented on Eqs. (25) and (26) (de Lima et al., 2010) and can be found with more details in the work from Ghanem and Spanos (1991).

For i and j odd, with $i \geq 1$ *and* $j \geq 1$, *geometric domains* $\Omega_x = \left[-a, a\right]$, $\Omega_y = \left[-b, b\right]$:

$$\lambda_i = \frac{2c_1}{\omega_i^{\,2} + c_1^{\,2}}, \quad f_i\left(x\right) = \alpha_i\cos\left(\omega_i x\right) \tag{25.a}$$

$$\lambda_j = \frac{2c_2}{\omega_j^{\,2} + c_2^{\,2}}, \quad f_j\left(y\right) = \alpha_j\cos\left(\omega_j y\right) \tag{25.b}$$

where $\alpha_i = 1/\sqrt{a + \sin\left(2\omega_i a\right)/2\omega_i}$, $\alpha_j = 1/\sqrt{b + \sin\left(2\omega_j b\right)/2\omega_j}$, $c_1 = 1/L_{cor,x}$ and $c_2 = 1/L_{cor,y}$.

The roots ω_i and ω_j given by the solution of the transcendental functions:

$$c_1 - \omega_i\tan\left(\omega_i a\right) = 0,\ c_2 - \omega_j\tan\left(\omega_j b\right) = 0 \tag{25.c}$$

defined into the domains $\left[\left(i-1\right)\frac{\pi}{a},\left(i-\frac{1}{2}\right)\frac{\pi}{a}\right]$ and $\left[\left(j-1\right)\frac{\pi}{b},\left(j-\frac{1}{2}\right)\frac{\pi}{b}\right]$.

For i and j even, with $i \geq 2$ *and* $j \geq 2$*, geometric domains* $\Omega_x = [-a,a]$, $\Omega_y = [-b,b]$*:*

$$\lambda_i = \frac{2c_1}{\omega_i{}^2 + c_1{}^2}, \quad f_i(x) = \alpha_i \sin(\omega_i x) \tag{26.a}$$

$$\lambda_j = \frac{2c_2}{\omega_j{}^2 + c_2{}^2}, \quad f_j(y) = \alpha_j \sin(\omega_j y) \tag{26.b}$$

where $\alpha_i = 1/\sqrt{a - \sin(2\omega_i a)/2\omega_i}$, $\alpha_j = 1/\sqrt{b - \sin(2\omega_j b)/2\omega_j}$.

The roots ω_i and ω_j given by the solution of the transcendental functions:

$$\omega_i + c_1 \tan(\omega_i a) = 0 \,, \ \omega_j + c_2 \tan(\omega_j b) = 0 \tag{26.c}$$

defined into the domains $\left[\left(i - \frac{1}{2}\right)\frac{\pi}{a}, i\frac{\pi}{a}\right]$ and $\left[\left(j - \frac{1}{2}\right)\frac{\pi}{b}, j\frac{\pi}{b}\right]$.

After the determination of the KL method's parameters, it is possible to calculate elementary stochastics matrices, now function of random variables θ. Equations (27) and (28) represents how they are calculated.

$$\mathbf{M}^{(e)}(\theta) = \mathbf{M}^{(e)} + \sum_{r=1}^{n} \bar{\mathbf{M}}_r^{(e)} \xi_r(\theta) \tag{27}$$

$$\mathbf{K}^{(e)}(\theta) = \mathbf{K}^{(e)} + \sum_{r=1}^{n} \bar{\mathbf{K}}_r^{(e)} \xi_r(\theta) \tag{28}$$

where $\mathbf{M}^{(e)}$ and $\mathbf{K}^{(e)}$ are the deterministic matrices calculated by Eqs. (3) and (4). $\bar{\mathbf{M}}_r^{(e)}$ and $\bar{\mathbf{K}}_r^{(e)}$ are the elementary random matrices, computed according to Eqs. (29) and (30).

$$\bar{\mathbf{M}}_r^{(e)} = \xi_r(\theta) \int_{L_x} \int_{L_y} \sqrt{\lambda_r}\, f_r(x,y)\, \boldsymbol{N}(x,y)^T \boldsymbol{N}(x,y)\, dydx \tag{29}$$

$$\bar{\mathbf{K}}_r^{(e)} = \xi_r(\theta) \int_{L_x} \int_{L_y} \sqrt{\lambda_r}\, f_r(x,y)\, \dot{\boldsymbol{N}}(x,y)^T \mathbf{H}\, \dot{\boldsymbol{N}}(x,y)\, dydx \tag{30}$$

where L_x and L_y depends on the reference assumed on the finite elements method.

Finally, these elementary matrices are assembled by element's connectivity as shown before on Eqs. (5) and (6).

SINE'S FATIGUE CRITERION

Uniaxial fatigue criteria with zero mean can be obtained directly from the S-N diagram (also known as Wöhler diagram, (Budynas and Nisbett, 2011)). If the structure is subjected to multiaxial loadings, there are different methods of fatigue life estimation. The most accepted and efficient uses tensor invariants, usually the first invariant of the stress tensor (I_1) or the second invariant of the deviation tensor (J_2). Weber (1999) pointed out on his studies several criteria and noticed that the best results were obtained by Fogue's and Sines' criteria.

Fogue's criterion presented slightly better results than Sines' but requires three material properties on his formulation, making it very restrict. On the other hand, Sines' criterion uses octahedral plan as the maximum shear plane and its formulation is simple, reducing computational time and effort. It also needs only two material properties related to fatigue (alternate torsional ($t_{\_1}$) and alternate traction ($f_{\_1}$) fatigue resistance).

On his work, Sines (1959) established a coefficient called D_{Sines} that express the probability of fatigue failure. It is statistically calculated due to random loadings. So instead of calculating it directly, what is needed is its expected value, given by Eq. (31) (Lambert, 2007).

$$E[D_{Sines}] = \frac{E[\sqrt{J_{2,a}}] + \alpha E\left[p(t)\right]}{A} \tag{31}$$

where $\sqrt{J_{2,a}}$ is the estimation of the square root of the second deviation tensor invariant, *p(t)* is the hydrostatic stress, $A = t_{-1}$, $\alpha = \frac{3t_{-1}(R_m + f_{-1})}{f_{-1}R_m} - \sqrt{6}$ and R_m is the ultimate material's strength.

Li and de Freitas (2002) proposed a method of evaluating $\sqrt{J_{2,a}}$ using the minimum circumscribed ellipse method. This method can be expanded for five-dimension prismatic hull circumscribing the loading path of $\sqrt{J_{2,a}}$. Equation (32) is used to estimate its value (Lambert et al., 2010).

$$E\left[\sqrt{J_{2,a}}\right]=\sqrt{E\left[R_1\right]^2+E\left[R_2\right]^2+E\left[R_3\right]^2+E\left[R_4\right]^2+E\left[R_5\right]^2} \tag{32}$$

Each semi-axe R_i of the prismatic hull is obtained by Eq. (33).

$$E\left[R_i\right]\approx\lambda_{0,i}\left(\sqrt{2\ln N_p\left(\tilde{D}_i(t)\right)}+\frac{\gamma}{\sqrt{2\ln N_p\left(\tilde{D}_i(t)\right)}}\right),i=1,\ldots,5 \tag{33}$$

where $\lambda_{0,i}$ is the zero-order spectral moment, $\gamma=0.5772$ is the Euler-Mascheroni constant and $N_p\left(\tilde{D}_i(t)\right)$ is the number of maxima on the gaussian process $\tilde{D}_i(t)$, estimated by Eq. (34).

$$N_p\left(\tilde{D}_i(t)\right)=\frac{T}{2\pi}\sqrt{\frac{\lambda_{1,i}{}^2}{\lambda_{2,i}{}^2}},i=1,\ldots,5 \tag{34}$$

where $\lambda_{1,i}$ and $\lambda_{2,i}$ are the first and second order spectral moments obtained from stress PSDs, respectively.

RESULTS AND DISCUSSION

Three major tests were performed to simulate random effects concerning the thin plate. They considered thickness variations with 2%, 5% and 10% of uncertainty level over a three-sigma deviation from the mean for the Latin Hypercube (LHC) sampling (Florian, 1992). They will be denoted case 1, case 2 and case 3 respectively. The responses obtained for each one of the tests are the convergence analysis, FRF envelopes and the expectation for the Sine's fatigue criterion coefficient.

Convergence Analysis of the Stochastic Response

Before starting the simulations, a convergence analysis was performed via root-mean-square deviation (RMSD) of the FRFs obtained by the stochastic model. It made possible to estimate the optimal number of samples (n_S) considered in the Monte Carlo method (Rubinstein, 1981). Equation (35) shows how it is calculated.

$$RMSD(n_S)=\sqrt{\frac{1}{n_S}\sum_{i=1}^{n_S}\left|G(\omega)-\bar{G}(\omega)\right|^2} \tag{35}$$

After applying Eq. (35), the result is normalized by its mean. Presuming that case 3 is the one presenting more variation and a larger FRF envelope, it was used as reference for the application of the RMSD. Figure (2) presents the convergence plot for 10% thickness variation. At about $n_S=250$ samples a satisfactory convergence for the method is noted, so it is possible to set this value as an optimal number for LHC.

Frequency Response Function Envelope

In the sequence, Eq. (13) is used to obtain, for each one of the cases, FRF envelopes of the displacement by a unitary impulse loading applied and measured on the central node. These envelopes are composed by its maximum, mean and minimum values for each frequency in the range. It is important to note here that the deterministic model FRF must fit inside this envelope for the response to be coherent, so it is plotted together with the random results as seen on Fig. (3).

As expected, with an increase of the uncertainty level for each case, the envelope became wider. Inside each one of them are the expected values used in order to obtain stress responses and fatigue analysis, as shown before on Eqs. (19) and (20). It is important to note here the difference between the mean values and the deterministic values. The first set is obtained by the first statistic moment of the random results while the second set is calculated by the system without any random effect, only based on mass and stiffness matrices presented in Eqs. (3) and (4).

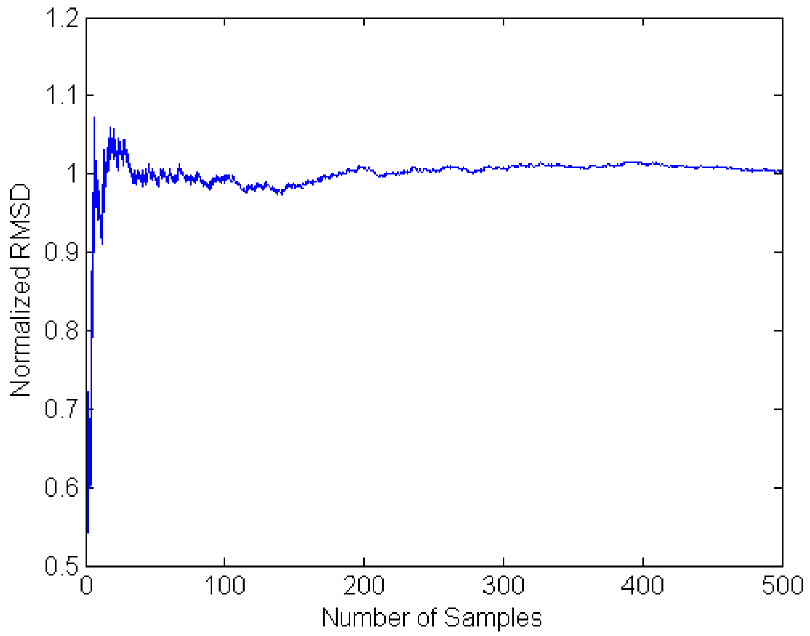

Figure 2. Convergence analysis via RMSD for case 3 (10% uncertainty level)

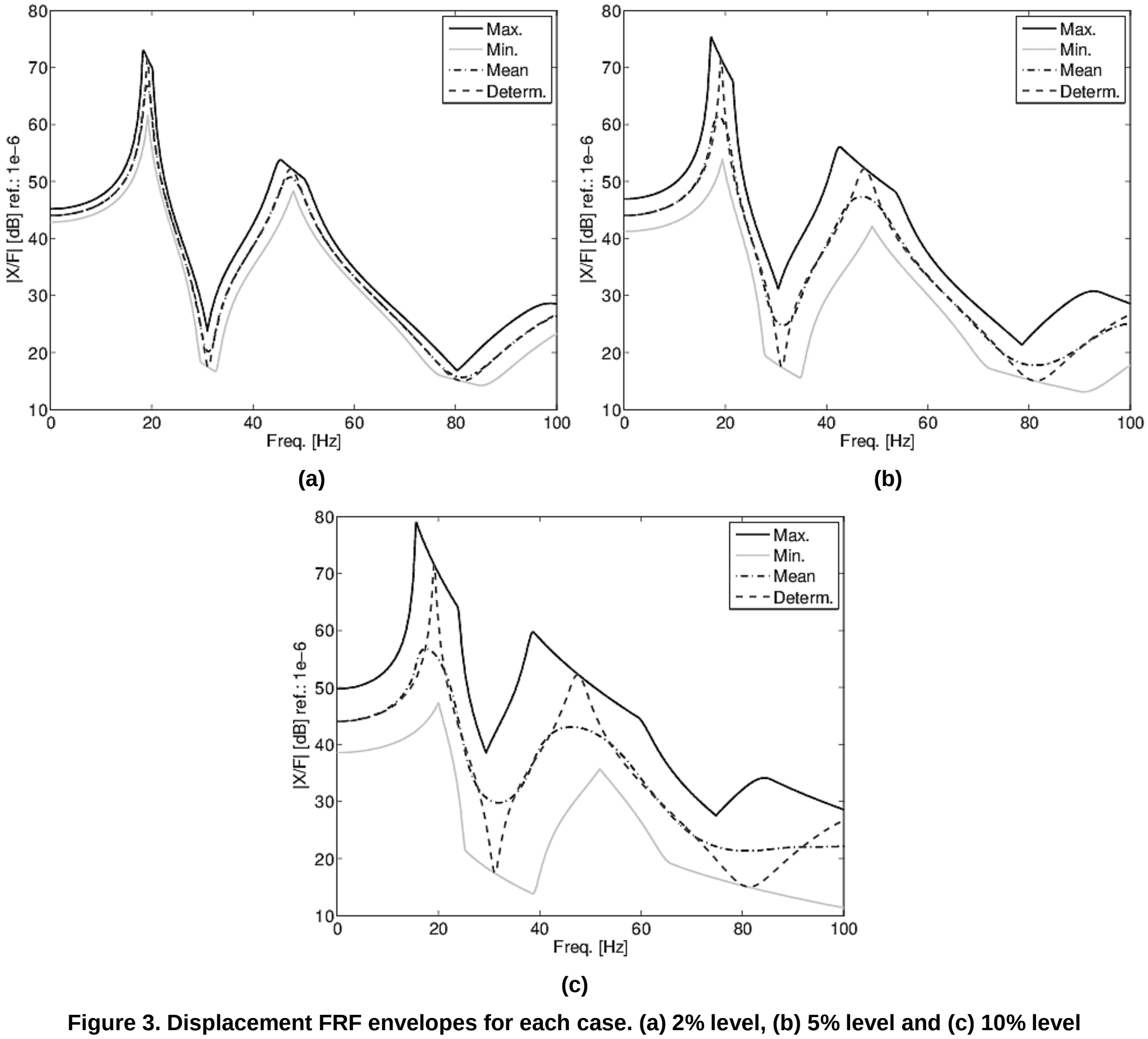

Figure 3. Displacement FRF envelopes for each case. (a) 2% level, (b) 5% level and (c) 10% level

Stochastic Fatigue Analysis

The last part of the stochastic analysis consists in obtaining Sine's fatigue coefficient expectation for each element of the plate, using Eq. (31). The loading applied is a white Gaussian noise with $\phi_f = 85\times10^3 Pa^2/Hz$ in the central node.

For all cases, the clamped border and central elements presented the greatest values for $E\left[D_{Sines}\right]$. This is an expected result, because these elements are subjected to the higher stress levels on the structure. Table 2 presents the maximum values encountered on this test. For each case, three contour plots were obtained for the maximum, mean and minimum expected values of the coefficient. They are depicted on Fig. 4. Results for deterministic tests regarding this structure can be found in bibliographic reference (Rosa and de Lima, 2015).

Table 2. Sine's coefficient expectation maximum values for each case and set of results

Case 1 (2% uncertainty)			Case 2 (5% uncertainty)			Case 3 (10% uncertainty)		
	Border	**Center**		**Border**	**Center**		**Border**	**Center**
Maximum	0.8202	0.7455	**Maximum**	0.8243	0.7471	**Maximum**	0.8243	0.7471
Mean	0.8107	0.7371	**Mean**	0.8076	0.7335	**Mean**	0.7941	0.7198
Minimum	0.8001	0.7264	**Minimum**	0.7762	0.7059	**Minimum**	0.7314	0.6644

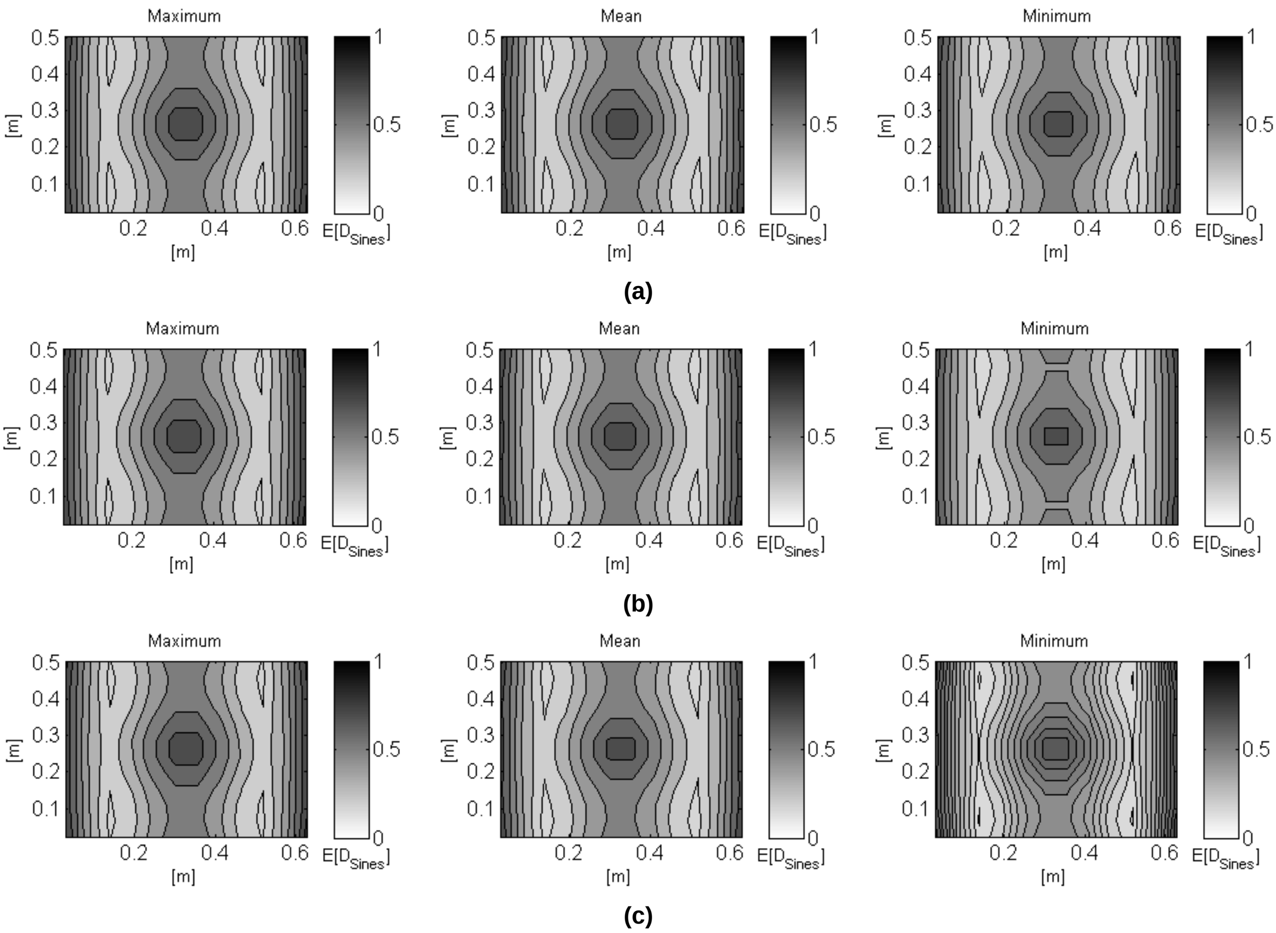

Figure 4. Sines coefficient distribution for each case. (a) 2% level, (b) 5% level and (c) 10% level

The exact stochastic modeling strategy concerning Karhunen-Loève expansions affecting directly mass and stiffness matrices combined with Sine's criterion application for a structure subjected to random loadings suggested in this work proved itself suitable for practical applications on fatigue damage estimation where efforts vary with time, such as relevant aerodynamic charging and supersonic vibration effects. Numerical simulations generating as final results contour plots with the statistical expectation for Sine's coefficient showed that it is possible to notice exactly which elements are more susceptible to failure after a certain number of cycles.

ACKNOWLEDGMENTS

The authors are grateful for Federal University of Uberlândia (UFU), Laboratório de Mecânica das Estruturas José Eduardo Tannus Reis (LMest) and Instituto Nacional de Ciência e Tecnologia de Estruturas Inteligentes em Engenharia (INCT-EIE) for the opportunity and support given to the realization of this research work and to CAPES (Coordenação de Aperfeiçoamento de Pessoal de Nível Superior), CNPq (Conselho Nacional de Desenvolvimento Científico e Tecnológico) and FAPEMIG (Fundação de Amparo à Pesquisa do Estado de Minas Gerais) for the financial support.

REFERENCES

Bendat, J. S. and Piersol, A.G., 2010. *Random Data: Analysis and Measurements Procedures*. John Wiley & Sons, New Jersey, 4th edition.

Budynas, R. G. and Nisbett, J. K., 2011. *Shigley's Mechanical Engineering Design*. McGraw-Hill, New York, 9th edition.

de Lima, A. M G., Rade, D. A. and Bouhaddi, N, 2010. "Stochastic modeling of surface viscoelastic treatments combined with model condensation procedures". *Shock and Vibration*, Vol. 17, p. 429-444.

Dowling, N. E., 2007. *Mechanical Behavior of Materials: Engineering Methods for Deformation, Fracture and Fatigue*. Pearson Prentice Hall, 3rd edition.

Faria, A. W., 2006. *Modelagem por elementos finitos de placas compostas dotadas de sensores e atuadores piezoelétricos: implementação computacional e avaliação numérica.* M.Sc. dissertation, UFU , Uberlândia, Brazil.

Florian, A., 1992. "An efficient sampling scheme: updates Latin Hypercube sampling". *Probabilistic Engineering Mechanics*, Vol. 7(2), p. 123-130.

Ghanem, R. G. and Spanos P. D., 1991. *Stochastic Finite Elements: A Spectral Approach*. Springer-Verlag, New York.

Gerges, Y., 2013. *Méthodes de reduction de modèles en vibroacoustique non-linéaire*. Ph.D. thesis, Université de Franche-Comté, Besançon.

Lambert, S., 2007. *Contribution à l'analyse d l'endommagement par fatigue et au dimensionnement de structures soumises à des vibrations aléatoires*. Ph.D. thesis, INSA de Rouen, Rouen.

Lambert, S., Pagnacco E. and Khalij, L., 2010. "A probabilistic model for the fatigue reliability of structures under random loadings with phase shift effects". *International Journal of Fatigue*, Vol. 32, p. 463-474.

Li, B. and de Freitas, M., 2002. "A procedure for fast evaluation of high-cycle fatigue under multiaxial random loading". *Journal of Mechanical Design*, Vol. 124, p. 558-563.

Rosa, U. L., de Lima, A. M. G., 2015. "Fatigue analysis of dynamic systems subjected to cyclic loading in the frequency domain". ABCM International Congress of Mechanical Engineering, Rio de Janeiro, Brazil.

Rubinstein, R. Y., 1981. *Simulation and the Monte Carlo Method*. John Wiley & Sons, New Jersey.

Sines, G., 1959. "Behavior of Metals Under Complex Static and Alternating Stresses", In *Metal Fatigue*, McGraw-Hill, New York.

Weber, B., 1999. *Fatigue multiaxiale des structures industrielles sous chargement quelconque*. Ph.D. thesis, INSA de Lion, Lion.

Zienkiewicz, O.C. and Taylor, R. L., 2005. *The Finite Element Method for Solid and Structural Mechanics*. Elsevier Butterworth-Heinemann, Oxford, 6th edition.

RESPONSIBILITY NOTICE

The authors are the only responsible for the material included in this paper.